ACS Catalysis

Research Article

pubs.acs.org/acscatalysis

Prospects for the Computational Design of Bipyridine *N,N′*-Dioxide Catalysts for Asymmetric Propargylation Reactions

Benjamin J. Rooks, Madison R. Haas, Diana Sepúlveda, Tongxiang Lu, and Steven E. Wheeler*

Department of Chemistry, Texas A&M University, College Station, Texas 77842, United States

Supporting Information

ABSTRACT: Stereoselectivities were predicted for the allylation of benzaldehyde using allyltrichlorosilanes catalyzed by 18 axially chiral bipyridine *N,N′*-dioxides. This was facilitated by the computational toolkit AARON (Automated Alkylation Reaction Optimizer for *N*-oxides), which automates the optimization of all of the required transition-state structures for such reactions. Overall, we were able to predict the sense of stereoinduction for all 18 of the catalysts, with predicted ee's in reasonable agreement with experiment for 15 of the 18 catalysts. Curiously, we find that ee's predicted from relative energy barriers are more reliable than those based on either relative enthalpy or free energy barriers. The ability to correctly predict the stereoselectivities for these allylation catalysts in an automated fashion portends the computational screening of potential organocatalysts for this and related reactions. By studying a large number of allylation catalysts, we were also able to gain new insight into the origin of stereoselectivity in these reactions, extending our previous model for bipyridine *N*-oxide-catalyzed alkylation reactions (*Organic Letters* **2012**, *14*, 5310). Finally, we assessed the potential performance of these bipyridine *N,N′*-dioxide catalysts for the propargylation of benzaldehyde using allenyltrichlorosilanes, finding that two of these catalysts should provide reasonable stereoselectivities for this transformation. Most importantly, we show that bipyridine *N,N′*-dioxides constitute an ideal scaffold for the development of asymmetric propargylation catalysts and, along with AARON, should enable the rational design of such catalysts purely through computation.

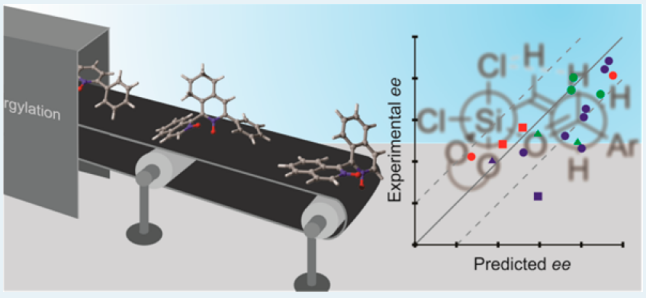

KEYWORDS: *organocatalysis, density functional theory, stereoselectivity, computational design, high-throughput screening*

I. INTRODUCTION

The field of organocatalysis continues to mature, and now provides efficient routes to many chiral synthetic building blocks without the need for transition-metal-based catalysts.[1−4] The rational design of stereoselective organocatalysts requires a detailed mechanistic understanding as well as a sound grasp of the underlying mode of asymmetric induction. To this end, computational quantum chemistry has emerged as an indispensable tool for understanding the sundry effects that govern the activity and stereoselectivity of these reactions, and can even facilitate the design of new asymmetric organocatalysts.[5−13] A key requirement for the purely computational design of organocatalysts is a means of automatically screening potential catalyst designs. In this way, many potential catalysts can be tested computationally, requiring only the most promising designs to be synthesized and tested experimentally. Although such computational screening in general is a daunting and largely unsolved problem, for certain classes of reactions, this is currently feasible. In particular, we show that the well-defined, chairlike six-member transition state (TS) structures of bidentate Lewis base-catalyzed alkylation reactions (Scheme 1) makes them ideal candidates for the automated computational prediction of stereoselectivities and, ultimately, computational catalyst design. This is made possible by the computational toolkit AARON (Automated Alkylation Reaction Optimizer for *N*-oxides), which will be described below for the first time.[14]

Scheme 1. Lewis Base-Promoted Allylation and Propargylation of Aromatic Aldehydes

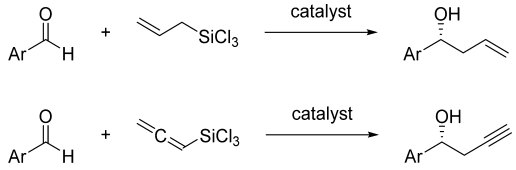

Synthetic routes to optically active homoallylic and homopropargyllic alcohols are highly desirable due to the utility of these building blocks in the synthesis of many complex chiral molecules.[5,15,16] Denmark and co-workers[17−24] pioneered a general strategy for the alkylation of aromatic aldehydes using alkyltrichlorosilanes catalyzed by bidentate Lewis base catalysts. This approach was further refined by Nakajima et al.[25,26] as well as Malkov and co-workers[27−31] in the context of allylation and propargylation reactions. Although these transformations can

Received: August 23, 2014
Revised: November 21, 2014
Published: November 24, 2014

   dx.doi.org/10.1021/cs5012553 | ACS Catal. 2015, 5, 272−280

follow different mechanisms depending on reaction conditions,[30,32] the generally accepted catalytic cycle for these reactions in solvents such as dichloromethane is shown in Figure 1. In this mechanism, the stereocontrolling transition

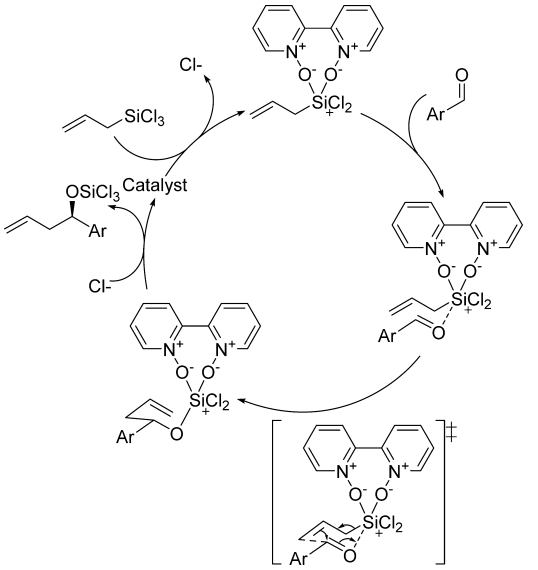

Figure 1. Catalytic cycle for the allylation of benzaldehyde using allyltrichlorosilane catalyzed by a bipyridine *N*,*N*′-dioxide catalyst.[25,31,35,36] The rate-limited and stereocontrolling transition state is depicted.

state follows the formation of a key hexacoordinate silicon intermediate and adopts a closed, chairlike geometry.[25,32−34] In this chairlike TS, the addition of the alkyl nucleophile (an allyl group or allenyl group for the allylation and propargylation reactions, respectively) to either the *Si* or *Re* face of the aldehyde results in formation of the (*S*)- or (*R*)-alcohols, respectively. Axially chiral bipyridine *N*,*N*′-dioxide catalysts are able to achieve stereoselectivity by inducing a difference in free energy between the lowest-lying transition states for these two competing pathways. That is, the preceding steps appear to be reversible, and stereoselectivity is entirely determined by the rate-limiting TS depicted in Figure 1.

Many bipyridine *N*,*N*′-dioxide catalysts have been developed that utilize this catalytic strategy for the allylation of benzaldehyde using allyltrichlorosilane (see Figure 2).[25,26,28,35−46] Moreover, many of these allylation catalysts exhibit high degrees of stereoselectivity (see Table 1). However, the development of related catalysts for the propargylation of benzaldehyde using the less reactive allenyltrichlorosilanes has proven much more difficult.[44] Indeed, there is only one example in the literature of a bipyridine *N*,*N*′-dioxide, developed by Nakajima et al.[26] in the late 1990s (catalyst **2**), that stereoselectively catalyzes the propargylation of aromatic aldehydes. Unfortunately, **2** provides only modest reactivity and stereoselectivity for propargylations (52% *ee*),[26] even though it is the most stereoselective of the bipyridine *N*,*N*′-dioxides for the allylation reaction.[25]

Discussions of the stereoselectivity of bidentate Lewis base-catalyzed alkylation reactions typically focus on a particular arrangement of the ligands around the hexacoordinate silicon. For example, Nakajima et al.[25] proposed a TS model in which the chlorines adopt a *cis* arrangement, the aldehyde is *trans* to

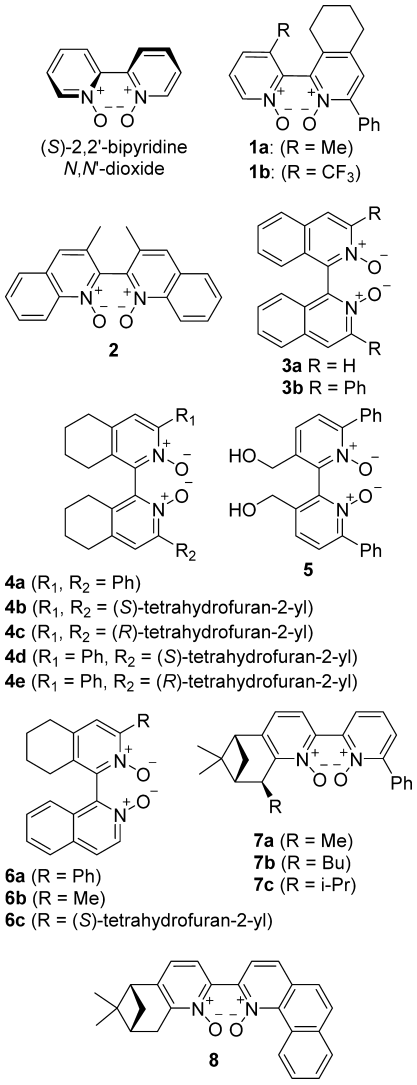

Figure 2. Bipyridine *N*,*N*′-dioxide catalysts for the allylation of benzaldehyde (**1** − **8**),[27,29,31,52−55] as well as the parent (*S*)-2,2′-bipyridine *N*,*N*′-dioxide. See Table 1 for computed and experimental.

one of the *N*-oxides, and the alkyl nucleophile is *trans* to a chlorine. More recently, many authors have invoked stereoelectronic arguments to justify TS models in which the chlorines adopt a *trans* arrangement and the alkyl nucleophile is positioned *trans* to one of the *N*-oxides in these and related reactions.[27,29,44,47] The latter model appears to be based at least in part on Denmark's work on bipyridine *N*,*N*′-dioxide-catalyzed aldol reactions.[48] However, we recently showed[49−51] that there are five viable ligand configurations for the hexacoordinate silicon intermediate in the case of bipyridine *N*,*N*′-dioxide-catalyzed alkylations (**BP1**-**BP5** in Figure 3). In the case of non-C_2-symmetric catalysts, there is a second possible orientation of the bidentate catalyst, giving rise to five additional configurations (**BP1**′-**BP5**′). From each of these intermediates, the alkyl nucleophile can add to either the *Si* or *Re* face of the aldehyde, leading to 10 (or 20 in the case of non-C_2-symmetric catalysts) transition states. These transition states are labeled by the ligand configuration (**BPX**) and whether they lead to the (*R*) or (*S*) alcohol. In general, any of these transition states can be low-lying,[49,50] although for bipyridine *N*,*N*′-dioxides, recent results indicate that transition states based on the ligand configuration **BP2** are often strongly

dx.doi.org/10.1021/cs5012553 | ACS Catal. 2015, 5, 272−280

Table 1. B97-D/TZV(2*d*,2*p*) Predicted and Experimental ee's (% *R*, Except Where Noted) for the Allylation of Benzaldehyde Catalyzed by 1−8[a]

		allylation					propargylation
cat	temp (K)	$\Delta\Delta E^{\ddagger}$	$\Delta\Delta H^{\ddagger}$	$\Delta\Delta G^{\ddagger}$	$\Delta\Delta G'^{\ddagger}$	expt	$\Delta\Delta E^{\ddagger}$
1a[b]	195	75	93	92	95	74 (ref 31)	66
1b[b]	195	89	95	96	97	72 (ref 31)	82
2[b]	195	93	92	93	93	88 (ref 25)	54[e]
3a[b]	296	72	73	84	79	52 (ref 31)	49
3b[b]	193	95	95	95	95	81 (ref 31)	88
4a[c]	233	82	85	90	87	65 (ref 52)	81
4b[c]	233	42	39	3	20	48 (ref 52)	29
4c[c]	233	80	86	97	93	46 (ref 52)	13[d]
4d[c]	195	59	60	59	60	53 (ref 53)	47
4e[c]	195	64	63	60	60	44 (ref 53)	50
5a[b]	195	76	90	90	91	80 (ref 54)	77
5b[b]	195	81	87	88	89	61 (ref 54)	56
5c[b]	195	78	89	94	95	49 (ref 52)	74
6[c]	228	91	88	82	86	84 (ref 55)	84
7a[b]	233	37	33	31	28	40 (ref 31)	68
7b[b]	233	55	38	15	21	56 (ref 31)	14
7c[b]	233	59	69	79	78	23 (ref 31)	61
8[b]	233	27	26	6[d]	14	42 (ref 31)	76
	MUE	12	16	25	22		
	max error	36	46	56	55		

[a]Values are based on relative energies ($\Delta\Delta E^{\ddagger}$), relative enthalpies ($\Delta\Delta H^{\ddagger}$), relative free energies ($\Delta\Delta G^{\ddagger}$), and relative quasi-RRHO free energies ($\Delta\Delta G'^{\ddagger}$), along with mean unsigned error (MUE) and maximum error, relative to experiment. Predicted ee's for the corresponding propargylation reactions are also provided. [b]Dichloromethane as solvent. [c]Acetonitrile as solvent. [d]Excess (*S*)-alcohol predicted. [e]Experimental ee is 52% (*R*) for the propargylation of benzaldehyde catalyzed by **2**.[26]

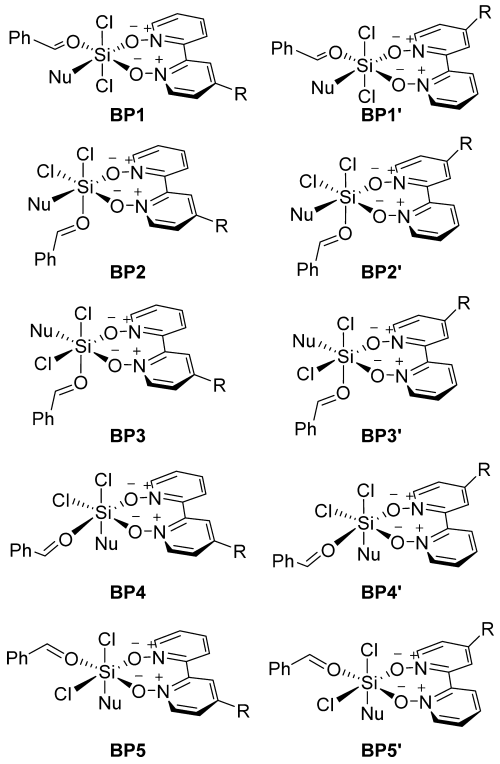

Figure 3. Ten possible ligand configurations for the hexacoordinate silicon intermediate preceding the stereocontrolling TS for bipyridine *N*,*N*′-dioxide-catalyzed alkylations of benzaldehyde.

favored over the others.[51] Nakajima's TS model[25] corresponds to **BP4**(*R*), whereas other popular TS models have been based on **BP1**/**BP1**′.[27,29,44,47]

Remarkably, the stereoselectivity of these catalysts is determined primarily by the arrangement of ligands about the central silicon atom.[49−51] That is, the stereoselectivity of a given bipyridine *N*-oxide or *N*,*N*′-dioxide catalyst is largely a consequence of which ligand configuration is low-lying for that particular catalyst. This is a consequence of the inherent bias of most of these ligand configurations toward the formation of either the (*R*) and (*S*) alcohol.[49−51] Moreover, a given ligand configuration is typically less inherently stereoselective for propargylations than it is for allylations, which presumably underlies the dearth of highly stereoselective bipyridine *N*-oxide and *N*,*N*′-dioxide propargylation catalysts.[49]

Although our previous studies[49−51] provided insights into the origin of stereoselectivity in *N*-oxide and *N*,*N*′-dioxide-catalyzed alkylation reactions, they were based on individual examples of these catalysts. This was due to the large number of TS structures that needed to be computed for each system. Here, we test the validity of our previous findings[49−51] on a significantly larger selection of bipyridine *N*,*N*′-dioxides, showcasing the utility of AARON[14] for the computational screening of bidentate Lewis base catalysts for asymmetric alkylation reactions. We also assessed the stereoselectivities of **1**−**8** in propargylation reactions. The results unveil two existing catalysts predicted to exhibit a relatively high degree of stereoselectivity for this transformation and also suggest that bipyridine *N*,*N*′-dioxides provide a more promising platform than *N*-oxides for the computational design of highly stereoselective propargylation catalysts.

II. THEORETICAL METHODS

All geometry optimizations and vibrational frequencies were performed at the B97-D/TZV(2*d*,2*p*) level of theory[56−58] using the PCM model to account for solvent effects.[59−61] This level

dx.doi.org/10.1021/cs5012553 | ACS Catal. 2015, 5, 272−280

of theory was previously shown to provide reliable predictions for bipyridine *N*,*N*′-dioxide-catalyzed allylations and propargylations[51] and lead to ee's in good agreement with experiment[29,44] for previously studied bipyridine *N*-oxide-catalyzed alkylation reactions.[49,50] We explored the prediction of ee's based on several different solution-phase quantities. First, ee's were predicted from free energy barriers evaluated within the standard rigid-rotor/harmonic oscillator (RRHO) approximations ($\Delta G^{\ddagger}$). We also considered ee's derived from free energies computed using the quasi-RRHO approach recently introduced by Grimme,[62] denoted by $\Delta G'^{\ddagger}$. In the quasi-RRHO approach, the entropic contribution of vibrational modes with frequencies less than 100 cm^{-1} are interpolated between the values of a harmonic oscillator and an effective rigid rotor. Finally, ee's were predicted based solely on enthalpy barriers, $\Delta H^{\ddagger}$, or energy barriers, $\Delta E^{\ddagger}$.[63] In each case, we considered a Boltzmann weighting of all possible (*R*) and (*S*) transition state structures, as was done previously.[49−51]Catalysts **7**−**8** do not have well-defined axial chirality due to the expected facile interconversion of the (*S*) and (*R*)-axially chiral forms. This complicates the prediction of the stereoselectivities, because the operative TS structures could feature the catalyst in either of the two axially chiral conformations. Consequently, in these cases, we computed 40 possible transition states for each catalyst for each reaction—20 corresponding to the (S)-chiral form (as was done for catalysts **1**−**6**) in addition to 20 for the (*R*)-chiral form of the catalyst. The predicted ee's were then based on a Boltzmann weighting of all 40 possible TS energies, enthalpies, or free energies.

Finally, we note that the bipyridine *N*,*N*′-dioxides in Figure 2 are relatively rigid, so they do not introduce the same complications encountered in more conformationally flexible catalytic systems. Regardless, some of these systems exist in multiple conformers. Data presented are based on the lowest-lying conformer located for each transition state structure.

A. AARON. For each of the catalysts in Figure 2, structures for 10 (for C_2-symmetric catalysts) or 20 (for nonsymmetric catalysts) possible transition states must be optimized to ensure proper identification of the lowest-lying transition states leading to the (*R*) and (*S*) alcohols.[64] Thus, the prediction of stereoselectivies of allylations and propargylations catalyzed by these 18 catalysts formally requires the optimization of 820 transition-state structures.[65] This would be a daunting and error-prone task to complete using conventional techniques. Consequently, the optimization of these TS structures was carried out in an automated fashion using AARON.[14] Briefly, AARON, through a text-based interface with Gaussian 09,[66] performs a hierarchical series of constrained and unconstrained optimizations on TS structures built by analogy with the transition states from the parent catalyst, (*S*)-2,2′-bipyridine *N*,*N*′-dioxide.[51] More precisely, AARON follows a protocol consisting of the following steps:

1. Input of catalyst structure and specification of reaction conditions (solvent, temperature, reaction type, etc.)
2. Construction of initial TS structures by mapping the proposed catalyst onto the parent (*S*)-2,2′-bipyridine *N*,*N*′-dioxide in precomputed TS structures for model reactions
3. Semiempirical geometry optimization of initial TS structures with constraints on all noncatalyst atoms to relieve steric interactions
4. DFT geometry optimization of structures with constrained forming C−C and breaking C−Si bond lengths, followed by DFT optimizations of the forming C−C and breaking C−Si bonds with the coordinates of all other atoms in the system frozen
5. Unconstrained DFT geometry optimization and vibrational frequency computation to confirm identity of TS structure via projection of normal vibrational modes onto those for model TS structures
6. Computation of relative energy, enthalpy, and free energy barriers, as well as prediction of ee's

Notably, all steps beyond 1 are fully automated, and extensive error checks are performed to ensure that the correct TS structures have been located.[67] This enables relatively rapid and almost entirely "hands-free" predictions of stereoselectivities for a large number of potential catalysts.[68] Presently, the semiempirical geometry optimizations are carried out using PM6,[69] whereas the DFT optimizations and frequencies are executed at the B97-D/TZV(2*d*,2*p*) level of theory.[56−58] As shown below, this dispersion-corrected DFT method, when paired with the PCM solvent model and the TZV(2*d*,2*p*) basis set, provides reasonably reliable predictions of experimental ee's for a broad range of bipyridine *N*,*N*′-dioxide-catalyzed allylation reactions.[27,29,31,52−55] We also considered ee's based on SMD-B97-D/TZV(2d,2p),[56−58,70] PCM-M06-2*X*/6-31+G(*d*),[71] SMD-M06-2*X*/6-31+G(*d*), and PCM-ωB97X-D/TZV-(2*d*,2*p*)[72] energies evaluated at the B97-D optimized geometries. All of these approaches lead to predicted ee's that are in far worse agreement with experiment than the PCM-B97-D data presented in Table 1 (see Supporting Information (SI) Table S1). Furthermore, evaluation of gas-phase B97-D energies computed at the solution-phase B97-D geometries lead to ee's there were in absolutely terrible agreement with experiment, highlighting the necessity of accounting for solvent effects in these reactions.

AARON is currently suited to predict the stereoselectivity for any bidentate Lewis base-catalyzed reaction that follows the mechanism shown in Figure 1 and for which the indicated TS is stereocontrolling. In particular, AARON has been tested for a range of bidentate Lewis base catalysts for allylations, crotylations, propargylations, and aldol reactions, and should provide a powerful tool for the automated screening of potential organocatalysts for any of these reactions. Here, we consider only allylations and propargylations catalyzed by bipyridine *N*,*N*′-dioxides. Applications of AARON to other reaction types will be discussed in future work. We emphasize that all semiempirical and DFT computations were carried out using Gaussian 09,[66] and employed density-fitting techniques when possible. AARON interfaces with Gaussian to construct initial TS structures, build input files, parse output files, and submit and monitor the prescribed geometry optimization and vibrational frequency computations for all TS structures.

III. RESULTS AND DISCUSSION

We have assessed the ability of B97-D/TZV(2*d*,2*p*) to predict the stereoselectivities of the bipyridine *N*,*N*′-dioxide catalysts depicted in Figure 2. Experimental ee's are available for all of these catalysts for the allylation of benzaldehyde, using either dichloromethane or acetonitrile as solvent and a range of different reaction temperatures (see Table 1). To our knowledge, published data is available for the stereoselectivity of only one of these catalysts (**2**) for the corresponding

dx.doi.org/10.1021/cs5012553 | ACS Catal. 2015, 5, 272−280

propargylation reaction.[26] These catalysts exhibit a broad range of stereoselectivities for allylations, going from the non-stereoselective **7c** (23% ee) to highly stereoselective catalysts such as Nakajima's catalyst, **2** (88% ee).[25] In the experimentally tested catalysts, the bipyridine *N,N′*-dioxides exhibit both (*R*)- and (*S*)-axial chirality. For catalysts **1**−**6**, we consider the (*S*)-chiral form of each of these catalysts in order to simplify comparisons among catalysts and so that all catalysts can be related to a single parent catalyst, (*S*)-2,2′-bipyridine *N,N′*-dioxide (Figure 2). Experimentally, the (*S*)-form of bipyridine *N,N′*-dioxides leads to excess formation of the (*R*)-homoallylic alcohol in all cases, as has been noted previously by Malkov and co-workers.[31] Similarly, experimental ee's for **7a**−**7c** and **8** are for the enantiomers of the structures shown in Figure 2, and lead to excess formation of the (*S*)-alcohol. We consider the forms of these catalysts depicted in Figure 2 so that all systems studied lead to excess formation of the (*R*)-alcohol. For **7a**−**7c** and **8**, we found that the (*S*)-axially chiral conformer lead to the lowest-lying TS structures.

A. Allylation Reactions. B97-D predicted stereoselectivities for the allylation of benzaldehyde catalyzed by the 18 bipyridine *N,N′*-dioxides in Figure 2 are compared with the corresponding experimental data in Table 1. First, regardless of how the ee's were computed, the overall (*R*) or (*S*) selectivity of these catalysts was predicted correctly in all but one case.[73] Surprisingly, ee's predicted based on relative energies are significantly more reliable than those from relative enthalpies or free energies. This is true even if the quasi-RRHO approximation of Grimme is employed.[62] That is, even though the quasi-RRHO approximation[62] provides some improvement over standard RRHO free energies, completely neglecting entropic and zero-point vibrational effects ultimately leads to smaller mean unsigned errors in predicted ee's for these systems. Consequently, solution-phase energy barriers will be considered exclusively below.

Predicted ee's based on relative energies are plotted against experimental data in Figure 4. These predicted ee's provide qualitative agreement with experiment, with a mean unsigned error (MUE) of 12%. In general, the predicted ee's tend to overestimate the stereoselectivity of these catalysts, compared to experiment. Computationally predicted ee's often overestimate experimentally stereoselectivities,[41,74,75] and, often, only the overall sense of stereoinduction or trend in stereoselectivities can be correctly predicted. However, for these allylation reactions, the overestimation is fairly minor, with the predicted ee's falling within 20% of the experimental data for 15 of the 18 catalysts considered. Moreover, for many of these catalysts, the predicted ee's are in very good agreement with experiment. In particular, for catalysts **1a**, **2**, **5**, **7a**, and **7b**, the predicted ee is within 5% of the experimental value, while the predictions are accurate to 10% for many others. Overall, B97-D/TZV(2*d*,2*p*), paired with AARON, provides reliable predictions of the stereoselectivity of these catalysts, and should be useful for the qualitative screening of potential bipyridine *N,N′*-dioxides for asymmetric alkylation reactions.

B. Origin of Stereoselectivity in Bipyridine *N,N′*-Dioxide Catalyzed Allylations. Next, we turn to the more general question of the origin of stereoselectivity in *N,N′*-dioxide-catalyzed allylation reactions. The examination of a large number of allylation catalysts provides a much more complete view of the stereoselectivity of these alkylation reactions than was available previously.[49−51] For each of the possible ligand configurations in Figure 3, there are chairlike

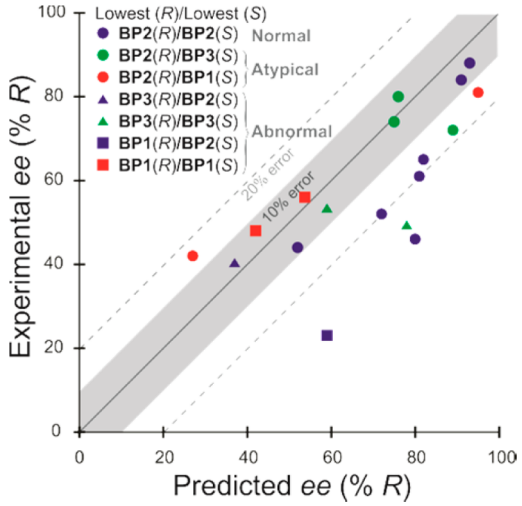

Figure 4. Experimental vs predicted ee's for the allylation of benzaldehyde catalyzed by **1** − **8**. The shapes of the points indicate which ligand configuration is low-lying for the (*R*) pathway, whereas the colors indicate the low-lying configuration of the (*S*) pathway for each catalyst (*n.b.* **BPX** and **BPX′** are grouped together for this purpose). For all catalysts, the (*R*) pathway is the global minimum. The solid line has a slope of one, whereas the gray shaded region denotes points within 10% of the experimental value and the dashed gray lines demarcate points within 20% of experiment.

transition states leading to both the (*R*) and (*S*) alcohol in which the aryl group on the aldehyde adopts an equatorial position (e.g., see Figure 5). Although each of these ligand configurations is technically feasible, we find that there are several strongly favored ligand configurations for bipyridine *N,N′*-dioxide-catalyzed allylations. In particular, **BP2**(*R*) [or **BP2′**(*R*)] is the lowest-lying TS structure for 12 of the 18 catalysts studied (circles in Figure 4). For the six exceptions, either **BP1**(*R*)/**BP1′**(*R*) or **BP3**(*R*)/**BP3′**(*R*) is favored. This is consistent with our previous work on catalyst **2**, as well as the parent catalyst (*S*)-bipyridine *N,N′*-dioxide (see Table 2).[51] However, we now have overwhelming evidence that **BP2**(*R*)/**BP2′**(*R*) is the most favorable TS for a wide range of (*S*)-bipyridine *N,N′*-dioxide catalysts. Curiously, apart from our recent work,[49−51] **BP2** has not been previously proposed as a likely, or even viable, ligand arrangement for these reactions. Instead, previous TS models have invoked the ligand configurations **BP1** or **BP4**, which appear to rarely play a role in bipyridine *N,N′*-dioxide-catalyzed allylation reactions.

There is much more variability in the case of the lowest-lying (*S*) transition state, which makes devising a general TS model for these reactions somewhat problematic. In particular, **BP2**(*S*) or **BP2′**(*S*) are the lowest-lying (*S*) transition states for only nine of the 18 catalysts (blue shapes in Figure 4), while the others are distributed uniformly across **BP1**(*S*)/**BP1′**(*S*) and **BP3**(*S*)/**BP3′**(*S*) (red and green shapes in Figure 4, respectively). Notably, for many of these catalysts, the ligand configuration in the operative TS for the (*R*) pathway is qualitatively different from that of the (*S*) pathway. This possibility has not previously been discussed for these or related reactions, but is not unreasonable based on computed energies for the parent catalyst, (*S*)-2,2′-bipyridine *N,N′*-dioxide.[51] That is, for this simple catalyst, **BP1**(*S*) and **BP3**(*S*) are only 0.7 and 0.1 kcal mol^{-1} higher in energy than **BP2**(*S*) (see Table 2), so it is unsurprising that they are low lying for some catalysts.

dx.doi.org/10.1021/cs5012553 | *ACS Catal.* 2015, 5, 272−280

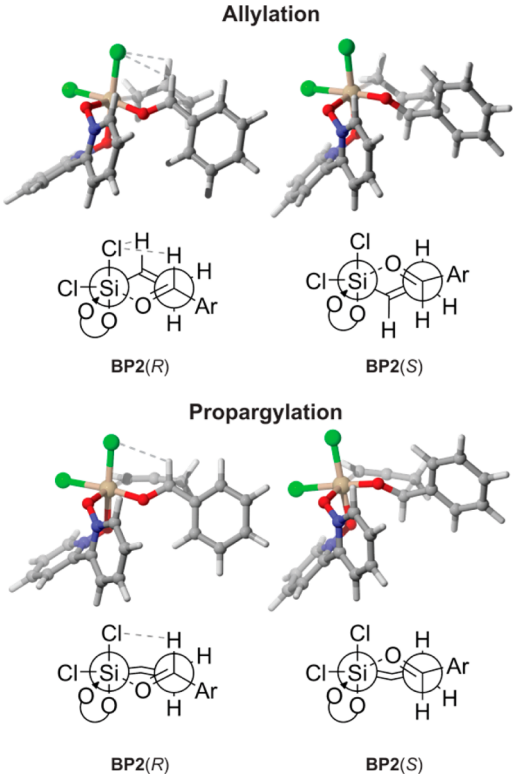

Figure 5. Optimized structures of the lowest-lying (*R*) and (*S*) transition states for "normal" allylation and propargylation catalysts, along with dual Newman projections looking down the forming C−C and breaking C−Si bonds. The favorable 1,3-diaxial interactions that preferentially stabilize **BP2**(*R*) over **BP2**(*S*) are indicated with gray dashed lines.

It is useful to classify bipyridine *N*,*N*′-dioxide catalysts based on the identity of the low-lying (*R*) and (*S*) transition states (see Figure 6). In particular, "normal" will refer to catalysts for which **BP2**(*R*)/**BP2**′(*R*) and **BP2**(*S*)/**BP2**′(*S*) are the lowest-lying transition states leading to the (*R*) and (*S*) alcohols, respectively (blue circles in Figure 4). Such catalysts will be most amenable to rational design, due to the involvement of only one type of ligand configuration in determining the stereoselectivity. "Atypical" catalysts are those for which **BP2**(*R*)/**BP2**′(*R*) is the lowest-lying (*R*) transition state, but the (*S*) pathway goes through either **BP1**(*S*)/**BP1**′(*S*) or **BP3**(*S*)/**BP3**′(*S*), as denoted by the red and green circles in Figure 4. Finally, "abnormal" will refer to the other cases in which **BP2**(*R*) is not the lowest-lying TS (the squares and triangles in Figure 4).

For normal allylation catalysts, the origin of stereoselectivity is fairly simple and arises from the difference in energy between **BP2**(*R*) and **BP2**(*S*). This follows results from the parent (*S*)-2,2′-bipyridine *N*,*N*′-dioxide, and stems primarily from attractive 1,3-diaxial interactions within the chairlike TS structure. In particular, in **BP2**(*R*), there are stabilizing electrostatic interactions between one of the chlorines and the two aligned C−H bonds (the central C−H of the allyl group as well as the aldehyde C−H, see Figure 5). These interactions are not present in **BP2**(*S*). The variation in ee's among normal catalysts arises from other interactions that further tune the energy of **BP2**(*S*), relative to **BP2**(*R*). Our hope is that these other interactions can be harnessed to further increase the energy separation between **BP2**(*S*) and **BP2**(*R*),

Table 2. Relative Energies (in kcal mol^{-1}) for the Possible Pairs of (*R*) and (*S*) Transition States for the Allylation and Propargylation of Benzaldehyde Catalyzed by the Parent Catalysts (*S*)-2,2′ Bipyridine *N*-oxide and (*S*)-2,2′ Bipyridine *N*,*N*′-dioxide, as well as the Difference in Energy between the (*R*) and (*S*) Transition States for Each Ligand Configuration, BPX[a]

	bipyridine *N*-oxide			bipyridine *N*,*N*′-dioxide		
	(*R*)	(*S*)	diff.	(*R*)	(*S*)	diff.
			allylation			
BP1	0.5	0.0	−0.5	2.0	2.1	0.1
BP2	0.2	2.5	2.3	0.0	1.4	1.4
BP3	4.1	0.1	−4.0	6.9	1.5	−5.4
BP4	8.4	3.4	−5.0	6.0	4.5	−1.5
BP5	5.1	7.2	2.1	5.0	8.4	3.5
BP1′	4.1	2.6	−1.5			
BP2′	0.4	2.1	1.7			
BP3′	6.5	1.8	−4.8			
BP4′	3.4	2.4	−1.0			
BP5′	1.1	6.7	5.6			
			propargylation			
BP1	0.3	0.0	−0.3	1.3	1.7	0.4
BP2	3.4	0.3	−3.0	0.0	0.9	0.9
BP3	0.4	0.9	0.6	6.4	1.2	−5.1
BP4	4.4	3.8	−0.6	5.1	4.7	−0.4
BP5	5.4	4.5	−1.0	3.2	3.8	0.5
BP1′	2.6	4.0	1.4			
BP2′	5.5	0.7	−4.8			
BP3′	0.7	2.1	1.4			
BP4′	0.6	5.8	5.1			
BP5′	3.6	2.7	−0.9			

[a]Energies evaluated at the PCM-B97-D/TZV(2*d*,2*p*) level of theory, with dichloromethane as solvent. Note that free energies for these systems were previously provided in refs 50 and 51, although the naming scheme used here for the *N*-oxide differs from that in ref 50 (see SI for naming of *N*-oxides).

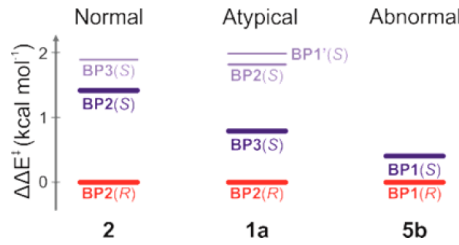

Figure 6. Relative energies of low-lying transition states for representative normal (**2**), atypical (**1a**), and abnormal (**5b**) allylation catalysts. The stereoselectivity in each case is primarily dependent on the energy difference between the lowest-lying (*R*) and (*S*) transition states (bold).

leading to highly stereoselective bipyridine *N*,*N*′-dioxide catalysts for asymmetric propargylations.

For the atypical and abnormal catalysts, the origin of the stereoselectivity is much less clear, because the operative TS structures for the (*R*) and (*S*) pathways exhibit qualitatively different structures. In these cases, only ad hoc explanations of the selectivity of each individual catalyst seem possible at this time. Moreover, for the atypical catalysts, the explanation given for the normal catalysts no longer holds, because the favorable 1,3-diaxial interactions that stabilize **BP2**(*R*) are also present in **BP1**(*S*)/**BP1**′(*S*) and **BP3**(*S*)/**BP3**′(*S*). Consequently, there

dx.doi.org/10.1021/cs5012553 | *ACS Catal.* 2015, 5, 272−280

must be other effects responsible for the overall lower energy of **BP2**(*R*) relative to **BP1**(*S*)/**BP1**′(*S*) and **BP3**(*S*)/**BP3**′(*S*) in these atypical cases. Most likely, a combination of favorable dispersion interactions and unfavorable steric interactions, which will obviously differ on a case-by-case basis, result in perturbations of the energetic ordering of the various transition states, relative to the parent catalyst. Interestingly, although the present data suggest that there is no overwhelming trend relating the preferred (*S*) transition state and the stereoselectivity of a given catalyst, we note that for the two most stereoselective catalysts, **2** and **6**, **BP2**(*S*)/**BP2**′(*S*) is the favored (*S*) transition state.

C. Propargylation Reactions. Having established that B97-D provides reliable predictions of the stereoselectivities of bipyridine *N*,*N*′-dioxide-catalyzed allylations, we next assessed the stereoselectivities of these catalysts for propargylations. Predicted ee's for the propargylation reaction, based on solution-phase relative energies, are listed in Table 1. Of these catalysts, an experimental ee has been provided for only one example, Nakajima's catalyst **2**. As recently discussed,[51] catalyst **2** provides a lower degree of stereoselectivity for the propargylation than for the allylation (52% vs 88% ee).[25,26] This is captured by the methods used here (54% ee for the propargylation and 93% ee for the allylation). Moreover, this trend also holds for the other catalysts considered; the stereoselectivies for the propargylation reaction are generally lower than the corresponding values for the allylation. This corroborates our previous proposal[49] that propargylations are inherently less stereoselective than allylations, which can be explained in the case of normal catalysts by the lack of a central C−H bond in the allenyl group. That is, whereas there are two C−H bonds aligned with the Si−Cl bond in favorable TS structures for the allylation, only one such C−H bond is present in the analogous propargylation transition state (see Figure 5). With regard to the lowest-lying (*R*) and (*S*) pathways, we observed the same trend as seen for the allylations. That is, **BP2**(*R*) was low-lying for all but six of the catalysts for propargylations (see SI Table S1). However, only five of the catalysts exhibit normal ordering of the TS energies for propargylations, with 11 exhibiting atypical energy ordering.

Among the catalysts tested, there are two promising catalyst for asymmetric propargylations (**3b** and **6**), which are potentially promising candidates for stereoselective propargylation catalysts. More precisely, these catalysts could be used as starting points for the design of propargylation catalysts with enhanced selectivities.

From the broader perspective of catalyst design, additional insight can be gained through comparisons of the parent bipyridine *N*-oxide and *N*,*N*′-dioxide catalysts in the propargylation reaction. Relative energies for the possible transition states for the propargylation of benzaldehyde catalyzed by (*S*)-2,2′-bipyridine *N*-oxide and (*S*)-2,2′-bipyridine *N*,*N*′-dioxide are shown in Table 2. The most notable difference between these parent catalysts is that **BP1**(*S*) is the lowest-lying structure for this simple *N*-oxide catalyst, whereas **BP2**(*R*) is strongly favored for the *N*,*N*′-dioxide. Moreover, (S)-2,2′-bipyridine *N*,*N*′-dioxide itself is predicted to be stereoselective for the propargylation of benzaldehyde (76% ee), even without any other groups appended. This is not the case for the *N*-oxide (21% ee).

From the data in Table 2, we see that for the *N*,*N*′-dioxide, there is only one transition state, **BP2**(*S*), that is within 1 kcal mol^{-1} of the lowest-lying TS, **BP2**(*R*). This can be contrasted with the parent *N*-oxide, for which **BP1**(*R*), **BP3**(*R*), **BP3**(*S*), **BP2**′(S), **BP3**′(*R*), and **BP4**′(*R*) are all within 0.7 kcal mol^{-1} of the lowest-lying configuration, **BP1**(*S*). Thus, realistic bipyridine *N*-oxides are much more likely to exhibit atypical or even abnormal behavior, since any of these transition states could be low-lying. In the case of *N*,*N*′-dioxides, normal catalysts will be more common, and the development of a stereoselective propargylation catalyst will primarily require the introduction of effects that increase the free energy gap between **BP2**(*S*) and **BP2**(*R*) (assuming that this does not also lead to drastic stabilization of one of the other transition states). In the case of *N*-oxides, one would need to devise an approach that will preferentially stabilize one of the many low-lying TS structures, but not the others. Presumably, this would be a more challenging task. These factors, combined with the greater catalytic activity of *N*,*N*′-dioxides over their *N*-oxide counterparts demonstrated by Malkov and co-workers,[31] suggests that bipyridine *N*,*N*′-dioxides are a much more promising framework for the design of stereoselective propargylation catalysts. Incidentally, the same conclusions hold for *N*-oxide and *N*,*N*′-dioxide catalysts for allylation reactions; the parent *N*,*N*′-dioxide provides a much more favorable gap in energy between the lowest-lying TS structure, **BP2**(*R*), and the remaining structures, compared to the parent *N*-oxide.

IV. SUMMARY AND CONCLUDING REMARKS

We assessed the ability of PCM-B97-D/TZV(2*d*,2*p*) to predict the stereoselectivities of 18 bipyridine *N*,*N*′-dioxide catalysts for the asymmetric allylation of benzaldehyde. This was made possible by AARON,[14] which automated the optimization of the 820 possible transition states. Solution-phase energies computed at this level of theory successfully predict that the (*S*)-form of these axially chiral catalysts leads to preferential formation of the (*R*)-alcohol for all 18 catalysts. Furthermore, for 15 of the 18 catalysts, the DFT-predicted ee's are within 20% of the experimental data, while many predictions are within 10%. We also used AARON to assess the stereoselectivity of these allylation catalysts for the propargylation of benzaldehyde using allenyltrichlorosilanes. The data reveal two existing catalysts (**3b** and **6**, Figure 2) that are predicted to provide stereoselectivities in propargylations comparable to the helical bipyridine *N*-oxide of Takenaka and co-workers[44] and exceeding that of the bipyridine *N*,*N*′-dioxide of Nakajima et al. (**2**).[26]

By examining the stereoselectivity of these bipyridine *N*,*N*′-dioxide catalysts in allylations and propargylations, we have also gained new insight into the origin of stereoselectivity in these reactions. In particular, for (*S*)-bipyridine *N*,*N*′-dioxide-catalyzed allylations and propargylations, a single TS is almost universally low-lying, **BP2**(*R*). However, there is considerable variability in the ligand configuration of the lowest-lying TS structure leading to formation of the (*S*)-alcohol. For "normal" catalysts, in which **BP2**(*R*) and **BP2**(*S*) are the lowest-lying TS structures for the (*R*) and (*S*) pathways, respectively, the stereoselectivity can be explained by favorable 1,3-diaxial interactions between C−H bonds and one of the Si−Cl bonds, which preferentially stabilize **BP2**(*R*) (see Figure 5).[13] Studies of the parent bipyridine *N*-oxide and *N*,*N*′-dioxide demonstrate that the latter provide greater energetic separation between **BP2**(*R*) and the other transition states, increasing the chances of achieving a "normal" energetic ordering of transition states. Such behavior will simplify catalyst design. This,

dx.doi.org/10.1021/cs5012553 | ACS Catal. 2015, 5, 272−280

combined with the established enhanced catalytic activity of *N*,*N*′-dioxides (compared to *N*-oxides),[31] suggests that the *N*,*N*′-dioxides will provide a superior platform for the rational development of catalysts for asymmetric propargylation reactions.

Overall, the stereoselectivity of bidentate Lewis base-catalyzed alkylation reactions are controlled by well-defined and relatively rigid transition state structures, making these transformations particularly amenable to rational, computational design of novel catalysts. We now have a powerful computational tool (AARON) for the qualitative screening of such designs.

■ ASSOCIATED CONTENT

Supporting Information

The following file is available free of charge on the ACS Publications website at DOI: 10.1021/cs5012553.

Additional data; absolute energies, enthalpies, and free energies; Cartesian coordinates (PDF)

■ AUTHOR INFORMATION

Corresponding Author

*E-mail: wheeler@chem.tamu.edu.

Notes

The authors declare no competing financial interest.

■ ACKNOWLEDGMENTS

This work was supported by The Welch Foundation (Grant A-1775) and the National Science Foundation (Grant CHE-1266022). We also thank the Texas A&M Supercomputing Facility for computational resources. Molecular structure figures were generated using CYLview.[76]

■ REFERENCES

(1) Dalko, P. I.; Moisan, L. *Angew. Chem., Int. Ed.* **2004**, *43*, 5138−5175.
(2) List, B.; Yang, J. W. *Science* **2006**, *313*, 1584−1586.
(3) Carpenter, J.; Northrup, A. B.; Chung, d.; Wiener, J. J. M.; Kim, S.-G.; MacMillan, D. W. C. *Angew. Chem., Int. Ed.* **2008**, *47*, 3568−3572.
(4) Dondoni, A.; Massi, A. *Angew. Chem., Int. Ed.* **2008**, *47*, 4638−4660.
(5) Bahmanyar, S.; Houk, K. N. *J. Am. Chem. Soc.* **2001**, *123*, 12911−12912.
(6) Allemann, C.; Gordillo, R.; Clemente, F. R.; Cheong, P. H.-Y.; Houk, K. N. *Acc. Chem. Res.* **2004**, *37*, 558−569.
(7) Clemente, F. R.; Houk, K. N. *Angew. Chem., Int. Ed.* **2004**, *43*, 5766−5768.
(8) Roy, D.; Sunoj, R. B. *Org. Lett.* **2007**, *9*, 4873−4876.
(9) Fleming, E. M.; Quigley, C.; Rozas, I.; Connon, S. J. *J. Org. Chem.* **2008**, *73*, 948−956.
(10) Houk, K. N.; Cheong, P. H.-Y. *Nature* **2008**, *455*, 309−313.
(11) Shinisha, C. B.; Sunoj, R. B. *Org. Biomol. Chem.* **2008**, *6*, 3921−3929.
(12) Shinisha, C. B.; Janardanan, D.; Sunoj, R. B. In *Kinetics and Dynamics*; Paneth, P., Dybala-Defratyka, A., Eds.; Springer: Dordrecht, The Netherlands, 2010; pp 107−136.
(13) Sunoj, R. B. *Wiley Interdisciplinary Reviews: Computational Molecular Science* **2011**, *1*, 920−931.
(14) Rooks, B. J.; Wheeler, S. E. *AARON*, version 0.3; Texas A&M University: College Station, TX, 2013.
(15) Marshall, J. A. *Chem. Rev.* **1996**, *96*, 31−48.
(16) Marshall, J. A. *J. Org. Chem.* **2007**, *72*, 8153−8166.
(17) Denmark, S. E.; Coe, D. M.; Pratt, N. E.; Griedel, B. D. *J. Org. Chem.* **1994**, *59*, 6161−6163.
(18) Denmark, S. E.; Fu, J. *J. Am. Chem. Soc.* **2000**, *122*, 12021−12022.
(19) Denmark, S. E.; Fu, J. *J. Am. Chem. Soc.* **2001**, *123*, 9488−9489.
(20) Denmark, S. E.; Wynn, T. *J. Am. Chem. Soc.* **2001**, *123*, 6199−6200.
(21) Denmark, S. E.; Fu, J. *Chem. Rev.* **2003**, *103*, 2763−2794.
(22) Denmark, S. E.; Fu, J.; Coe, D. M.; Su, X.; Pratt, N. E.; Griedel, B. D. *J. Org. Chem.* **2006**, *71*, 1513−1522.
(23) Denmark, S. E.; Pham, S. M.; Stavenger, R. A.; Su, X.; Wong, K.-T.; Nishigaichi, Y. *J. Org. Chem.* **2006**, *71*, 3904−3922.
(24) Denmark, S. E.; Beutner, G. L. *Angew. Chem., Int. Ed.* **2008**, *47*, 1560−1638.
(25) Nakajima, M.; Saito, M.; Shiro, M.; Hashimoto, S.-i. *J. Am. Chem. Soc.* **1998**, *120*, 6419−6420.
(26) Nakajima, M.; Saito, M.; Hashimoto, S. *Tetrahedron: Asymmetry* **2002**, *13*, 2449−2452.
(27) Malkov, A. V.; Bell, M.; Orsini, M.; Pernazza, D.; Massa, A.; Herrmann, P.; Meghani, P.; Kočovský, P. *J. Org. Chem.* **2003**, *68*, 9659−9668.
(28) Malkov, A. V.; Kočovský, P. *Eur. J. Org. Chem.* **2007**, *2007*, 29−36.
(29) Malkov, A. V.; Orsini, M.; Pernazza, D.; Muir, K. W.; Langer, V.; Meghani, P.; Kočovský, P. *Org. Lett.* **2002**, *4*, 1047−1049.
(30) Malkov, A. V.; Ramirez-Lopez, P.; Biedermannova, L.; Rulisek, L.; Dufková, L.; Kotora, M.; Zhu, F.; Kočovky, P. *J. Am. Chem. Soc.* **2008**, *130*, 5341−5348.
(31) Malkov, A. V.; Westwater, M.-M.; Gutnov, A.; Ramírez-López, P.; Friscourt, F.; Kadlčíková, A.; Hodačová, J.; Rankovic, Z.; Kotora, M.; Kočovský, P. *Tetrahedron* **2008**, *64*, 11335−11348.
(32) Hrdina, R.; Opekar, F.; Roithova, J.; Kotora, M. *Chem. Commun.* **2009**, 2314−2316.
(33) Chelucci, G.; Belmonte, N.; Benaglia, M.; Pignataro, L. *Tetrahedron Lett.* **2007**, *48*, 4037−4041.
(34) Sereda, O.; Tabassum, S.; Wilhelm, R. *Top. Curr. Chem.* **2010**, *291*, 349−393.
(35) Ding, C.-H.; Hou, X.-L. *Chem. Rev.* **2011**, *111*, 1914−1937.
(36) Barnett, D. S.; Schaus, S. E. *Org. Lett.* **2011**, *13*, 4020−4023.
(37) Jain, P.; Antilla, J. C. *J. Am. Chem. Soc.* **2010**, *132*, 11884−11886.
(38) Jain, P.; Wang, H.; Houk, K. N.; Antilla, J. C. *Angew. Chem., Int. Ed.* **2012**, *51*, 1391−1394.
(39) Reddy, L. R. *Org. Lett.* **2012**, *14*, 1142−1145.
(40) Chen, M.; Roush, W. R. *J. Am. Chem. Soc.* **2012**, *134*, 10947−10952.
(41) Grayson, M. N.; Pellegrinet, S. C.; Goodman, J. M. *J. Am. Chem. Soc.* **2012**, *134*, 2716−2722.
(42) Iseki, K.; Kuroki, Y.; Kobayashi, Y. *Tetrahedron: Asymmetry* **1998**, *9*, 2889−2894.
(43) Evans, D. A.; Sweeney, Z. K.; Rovis, T.; Tedrow, J. S. *J. Am. Chem. Soc.* **2001**, *123*, 12095−12096.
(44) Chen, J.; Captain, B.; Takenaka, N. *Org. Lett.* **2011**, *13*, 1654−1657.
(45) Chelucci, G.; Murineddu, G.; Pinna, G. A. *Tetrahedron: Asymmetry* **2004**, *15*, 1373−1389.
(46) Hosomi, A.; Sakurai, H. *J. Am. Chem. Soc.* **1977**, *99*, 1673−1675.
(47) Traverse, J. F.; Zhao, Y.; Hoveyda, A. H.; Snapper, M. L. *Org. Lett.* **2005**, *7*, 3151−3154.
(48) Denmark, S. E.; Fan, Y.; Eastgae, M. D. *J. Org. Chem.* **2005**, *70*, 5235−5248.
(49) Lu, T.; Porterfield, M. A.; Wheeler, S. E. *Org. Lett.* **2012**, *14*, 5310−5313.
(50) Lu, T.; Zhu, R.; An, Y.; Wheeler, S. E. *J. Am. Chem. Soc.* **2012**, *134*, 3095−3102.
(51) Sepulveda, D.; Lu, T.; Wheeler, S. E. *Org. Biomol. Chem.* **2014**, *12*, 8346−8353.
(52) Hrdina, R.; Dračínský, M.; Valterová, I.; Hodačová, J.; Císařová, I.; Kotora, M. *Adv. Synth. Catal.* **2008**, *350*, 1449−1456.

(53) Kadlčíková, A.; Hrdina, R.; Valterová, I.; Kotora, M. *Adv. Synth. Catal.* **2009**, *351*, 1279−1283.
(54) Hrdina, R.; Valterová, I.; Hodačová, J.; Císařová, I.; Kotora, M. *Adv. Synth. Catal.* **2007**, *349*, 822−826.
(55) Shimada, T.; Kina, A.; Ikeda, S.; Hayashi, T. *Org. Lett.* **2002**, *4*, 2799−2801.
(56) Becke, A. *J. Chem. Phys.* **1997**, *107*, 8554−8560.
(57) Grimme, S. *J. Comput. Chem.* **2006**, *27*, 1787−1799.
(58) Schafer, A.; Huber, C.; Ahlrichs, R. *J. Chem. Phys.* **1994**, *100*, 5829−5835.
(59) Cancès, E.; Mennucci, B. *J. Math. Chem.* **1998**, *23*, 309−326.
(60) Cancès, E.; Mennucci, B.; Tomasi, J. *J. Chem. Phys.* **1997**, *107*, 3032−3041.
(61) Tomasi, J.; Mennucci, B.; Cammi, R. *Chem. Rev.* **2005**, *105*, 2999−3093.
(62) Grimme, S. *Chem.—Eur. J.* **2012**, *18*, 9955−9964.
(63) Because these calculations were performed with PCM, these enthalpies and energies formally contain solvation free energy corrections, so are not purely enthalpies or energies. More precisely, by "relative enthalpies" we mean the sum of electronic energies plus zero-point vibrational energies, thermal corrections, and solvation free energy corrections, without entropic corrections. "Relative energies" refer to electronic energies plus solvation free energies.
(64) As noted above, for catalysts **7a**−**7c** and **8**, ee predictions require the computation of 40 TS structures.
(65) Some of these TS structures were not geometrically viable due to severe steric congestion. In total, the data presented in Table 1 are based on 674 optimized TS structures.
(66) Frisch, M. J.; Trucks, G. W.; Schlegel, H. B.; Scuseria, G. E.; Robb, M. A.; Cheeseman, J. R.; Scalmani, G.; Barone, V.; Mennucci, B.; Petersson, G. A.; et al. *Gaussian 09*, version D.01; Gaussian, Inc.: Wallingford, CT, 2009.
(67) One could envision various approaches to improve the efficiency of the above procedure. For example, currently, Hessians are explicitly computed preceding the unconstrained optimization in Step 5. However, we could instead project the normal modes from the reference TS onto an approximate Hessian.
(68) Presently, the computation of some TS structures for some catalysts require human intervention. This is primarily the case in sterically conguested structures, for which AARON is not always able to construct reasonable starting TS structures.
(69) Stewart, J. J. P. *J. Mol. Model.* **2007**, *13*, 1173−1213.
(70) Marenich, A. V.; Cramer, C. J.; Truhlar, D. G. *J. Phys. Chem. B* **2009**, *113*, 6378−6396.
(71) Zhao, Y.; Truhlar, D. G. *Theor. Chem. Acc.* **2008**, *120*, 215−241.
(72) Chai, J.-D.; Head-Gordon, M. *J. Chem. Phys.* **2008**, *128*, 084106.
(73) For catalyst **8**, the predicted ee based on relative free-energies is 6% ee (S), in conflict with the experimentally observed 42% ee (R).
(74) Dudding, T.; Houk, K. N. *Proc. Natl. Acad. Sci. U.S.A.* **2004**, *101*, 5770−5775.
(75) Grayson, M. N.; Goodman, J. M. *J. Am. Chem. Soc.* **2013**, *135*, 6142−6148.
(76) Legault, C. Y. *CYLView 1.0b*; Université de Sherbrooke, 2009 (http://www.cylview.org).